Chapter 22
Various Droop Control Strategies in Microgrids

Pegah Zafari, Ali Zangeneh, Mohammad Moradzadeh, Alireza Ghafouri and Moein Aldin Parazdeh

Abstract Droop control is a well-known strategy to control active power in power systems without internal communication. It is usually implemented on the conventional power plants to control the injected power of synchronous generators to the grid. As this strategy is local, there is no need to communication systems. Thus, it reduces the complexity and cost of the system operation and improves the reliability indices. Also, droop control has been used to control the active and reactive power of distributed generations in microgrids. Frequency and voltage control of microgrid and proper power sharing between DGs are the most important goals of droop control in the islanded mode of operation. The conventional droop control has some disadvantages that limits their application in the modern microgrids. Slow transient dynamics, load dependency of voltage and frequency, low accuracy on power sharing, low power quality for non-linear or unbalanced loads and circulating current between DGs are some of the main disadvantageous. Different methods have been proposed by researchers to overcome the problems, which are still an attractive subject for them. This chapter discusses different improved droop controllers, which have been used to overcome some of the problems.

Keywords Droop control · Microgrid · DG · Active/reactive power control

P. Zafari · A. Zangeneh · M. Moradzadeh (✉) · M. A. Parazdeh
Electrical Engineering Department, Shahid Rajaee Teacher Training University, Tehran, Iran
e-mail: m.moradzadeh@sru.ac.ir

P. Zafari
e-mail: p.zafari@sru.ac.ir

A. Zangeneh
e-mail: a.zangeneh@sru.ac.ir

M. A. Parazdeh
e-mail: parazdeh@sru.ac.ir

A. Ghafouri
Electrical Engineering Department, Sari Branch, Islamic Azad University (IAU), Sari, Iran
e-mail: ghafuriar@gmail.com

N. Mahdavi Tabatabaei et al. (eds.), *Microgrid Architectures, Control and Protection Methods*, Power Systems,
https://doi.org/10.1007/978-3-030-23723-3_22

22.1 Introduction

As a power plant, the droop characteristic can be implemented for DGs with appropriate control system. It is required that each DG has a control system to implement the droop characteristic [1–3]. Local implementation, no need to communication systems, easy expansion, acceptable reliability and low investment cost are some important benefits of droop controllers. Despite of the benefits, some of their shortcomings are:

a. Frequency and voltage deviations: In the islanded mode, the frequency and voltage of microgrid are highly sensitive to load changes. Increasing the slope of the droop characteristic improves the response of microgrid to the load changes but destroys the frequency and voltage regulation, as well as the stability of microgrid [4].
b. Harmonic loads: traditional droop control is appropriate for the basic load dispatch and it does not perform harmonic load dispatch among nonlinear loads. Low power quality and slow dynamic response are two important shortcomings of this control [5, 6].
c. Unknown and different line impedances: line impedances between parallel converters affects the power flow. Different impedances between inverters and point of common coupling leads to a large circulating current between inverters and decreases the accuracy of power dispatch [7, 8].
d. Output power oscillations of DGs: As the primary energy resources of renewable DGs are variable, the conventional droop cannot provide a smooth power for the microgrid [9].

In recent years, new studies have been performed to overcome the previous illustrated problems. In [10], a transformation matrix, which consider the line impedance in the calculation of droop parameters are presented to overcome the strong coupling between active and reactive power. To assess the stability of the microgrid with high penetration of renewable systems, a special droop control called virtual multi-slack has been introduced [11]. Peyghami et al. [12] propose a new droop control scheme for low voltage DC microgrid to avoid active power sharing errors by merging secondary voltage regulation and primary power sharing. In [13], an optimization method is introduced to find optimal droop parameters in the control mechanism. The information considered in [13] is not sufficient and determination of the optimal droop parameters are also dependent to microgrid stability [14].

In this chapter, we introduce various droop strategies and simulate some the prevalent ones to assess the strength and weakness of each approach.

22.2 Conventional Droop Control

This method is based on the conventional droop control of synchronous generators. The active and reactive power of each DG is determined regarding its nominal capacity and the droop coefficient. The droop coefficient plays the role of a virtual resistance regarding the grid side of DG inverters. Adjusting the droop coefficient changes the output resistance of DG inverters and controls the injected power of each DG to the grid. So the local controller of each DG should control the output characteristics of its inverter and it can be used for the frequency and voltage control of microgrid. Some controllers add a virtual series reactance to the power line in series with DGs. The output voltage and frequency of the inverter is controlled based on the reference active and reactive power of DGs, so the Q-V and P-f droop controllers are usually good candidates [15–17]. The typical equivalent circuit of a DG connected to the grid through its inverter has been shown in Fig. 22.1.

The injected active and reactive powers are derived by Eqs. (22.1)–(22.3).

$$S = P + jQ \tag{22.1}$$

$$P = \left(\frac{EV}{Z}\cos\varphi - \frac{V^2}{Z}\right)\cos\theta + \frac{EV}{Z}\sin\varphi\ \sin\theta \tag{22.2}$$

$$Q = \left(\frac{EV}{Z}\cos\varphi - \frac{V^2}{Z}\right)\sin\theta + \frac{EV}{Z}\sin\varphi\ \cos\theta \tag{22.3}$$

Considering Z as an imaginary reactance, Eqs. (22.2) and (22.3) can be simplified as:

$$P = \frac{EV}{X}\sin\varphi \tag{22.4}$$

$$Q = \frac{EV\cos\varphi - V^2}{X} \tag{22.5}$$

where, X, φ, E and V are the output reactance of inverter, the phase angle difference between the voltages of the inverter output and the PCC, the voltage magnitude of inverter bus and the voltage of PCC, respectively. The active power can be adjusted directly by φ and the reactive power by E. so the droop controller can be designed based on this relationship by Eqs. (22.6) and (22.7).

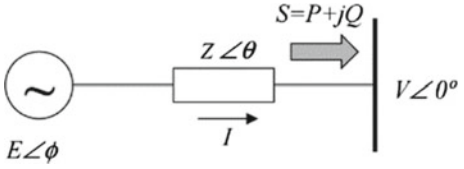

Fig. 22.1 Connection of DG to the AC bus [18]

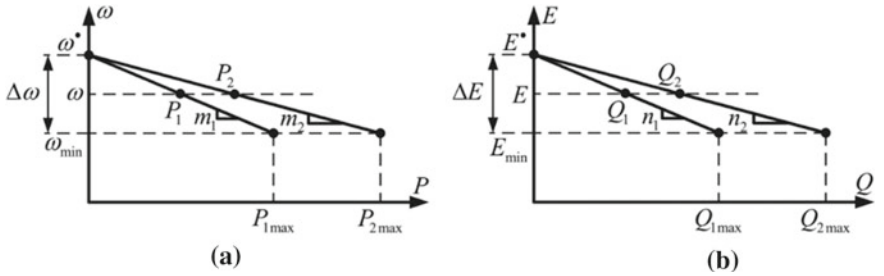

Fig. 22.2 Conventional droop characteristics [21]

$$\omega = \omega^* - mP \tag{22.6}$$

$$E = E^* - nQ \tag{22.7}$$

where, E^* and ω^* are the voltage and frequency references and E and ω are the output voltage and frequency of the inverter. n and m are the frequency and voltage droop coefficients defined by Eqs. (22.8) and (22.9) [19, 20].

$$m = \frac{f_i - f_{i\min}}{P_i - P_{i\max}} \tag{22.8}$$

$$n = \frac{E_{i\max} - E_{i\min}}{Q_{i\min} - Q_{i\max}} \tag{22.9}$$

Frequency and voltage droops have been shown in Fig. 22.2.

The conventional droop control has some disadvantages that limit their application in the modern microgrids. Some of the weaknesses are the slow transient dynamics, load dependency of voltage and frequency, low accuracy on reactive power sharing, low power quality for non-linear or unbalanced loads and circulating current between DGs [22].

In the conventional droop, reactive power sharing is not accurate due to highly dependency between line impedance and local load as well as the coupling between active and reactive power. Kosari and Hosseinian [23] proposed a reactive power compensation process (RCP) to resolve this problem. In this method, the error of reactive power sharing among DGs is compensated by simultaneously forming a transient coupling between active and reactive power and applying following droop equations in Eqs. (22.10) and (22.11) instead Eqs. (22.6) and (22.7). The reactive power term in Eq. (22.10) consider the reactive power sharing error in the P-f control and the third term in Eq. (22.11) consider the error in V-Q droop control by integrating during the transient coupling conditions.

$$\omega_i = \omega_0 - m_i P_i + G k_q (n_i Q_i) \tag{22.10}$$

$$E_i = E_0 - n_i Q_i + \frac{k_I}{s} G\left(P_{i,avg} - P_i\right) \tag{22.11}$$

where, k_q and k_I are respectively reactive power coefficient and integral gain, G is soft compensation gain which increases as a ramp at the beginning and decreases similarly at the end of compensation, $P_{i,avg}$ is the average active power in the steady state before load change.

22.3 Reverse Droop Control (*V-P* and *Q-F* Boost)

The conventional droop control of the previous section is appropriate for the high voltage transmission systems because of small line resistance respect to the line reactance. Unfortunately, it does not work for the low voltage microgrids with high resistive lines. The typical equivalent circuit of a DG connected with its inverter to the grid has been shown in Fig. 22.3 [24, 25].

The injected active and reactive powers are derived by Eqs. (22.1)–(22.3) [24].

$$P = \left(\frac{EV}{Z}\cos\varphi - \frac{V^2}{Z}\right)\cos\theta + \frac{EV}{Z}\sin\varphi\ \sin\theta \tag{22.12}$$

$$Q = \left(\frac{EV}{Z}\cos\varphi - \frac{V^2}{Z}\right)\sin\theta + \frac{EV}{Z}\sin\varphi\ \cos\theta \tag{22.13}$$

where, Z, θ, φ, E and V are respectively the magnitude of output impedance, impedance phase angle, the phase angle difference between the voltages of the inverter output and the PCC, the voltage magnitude of inverter bus and the voltage of PCC, respectively.

Considering Z as a resistive impedance, Eqs. (22.12) and (22.13) can be simplified as:

$$P = \frac{EV}{R}\cos\varphi - \frac{V^2}{R} \tag{22.14}$$

$$Q = -\frac{EV}{R}\sin\varphi \tag{22.15}$$

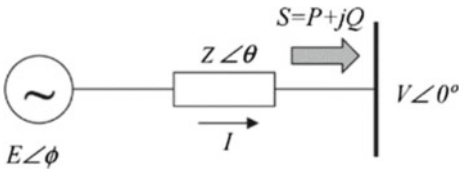

Fig. 22.3 Connection of DG to the AC bus [24]

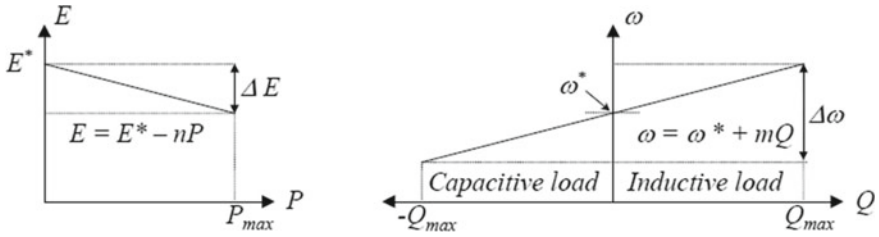

Fig. 22.4 Reverse droop control [25]

In a typical power system φ is approximately zero ($\cos\varphi \approx 1$, $\sin\varphi \approx \varphi$) and Eqs. (22.14) and (22.15) can be approximated as:

$$P \approx \frac{V}{R}(E - V) \tag{22.16}$$

$$Q \approx -\frac{EV}{R}\varphi \tag{22.17}$$

From Eqs. (22.16) and (22.17), it can be seen that the active power is proportional to the voltage of inverter bus and the reactive power decreases by increasing the phase angle. So droop characteristics should be defined by the curves in Fig. 22.4 and Eqs. (22.18) and (22.19) [25].

$$E_i = E^* - n \cdot P_i \tag{22.18}$$

$$\omega_i = \omega^* + m \cdot Q_i \tag{22.19}$$

where, m is the boost coefficient of the reactive power (Q) and n is the droop coefficient of the active power (P). Although this method improves the power sharing of low voltage microgrids including high resistive lines, its performance is highly dependent to the system parameters and has a weak response to the reactive power control [25].

22.4 Complex Line Impedance-Based Droop

The conventional droop control has a weak performance for the microgrids including complex impedance lines. To improve the dynamic response and exact power control of microgrid, some modified droop controllers should be utilized. The typical equivalent circuit of a DG connected with its inverter to the grid has been shown in Fig. 22.5 [18].

The injected current by DG to the grid can be derived from Eqs. (22.20) and (22.21).

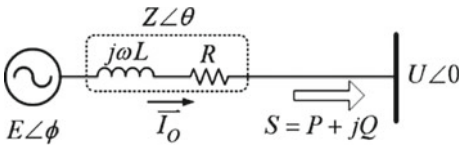

Fig. 22.5 Connection of DG to the AC bus [18]

Table 22.1 Active and reactive power with different types of system impedance [18]

System impedance	Pure inductive $\theta = 90,\ \bar{Z} = jX$	Pure resistive $\theta = 0°,\ \bar{Z} = R$	Complex impedance $\theta,\ \bar{Z} = R + jX$
Active power	$P \cong \frac{UE\varphi}{Z}$	$P \cong \frac{U(E-U)}{Z}$	$P \cong \frac{U}{Z}[(E-U)\cos\theta + E\varphi\sin\theta]$
Reactive power	$Q \cong \frac{U(E-U)}{Z}$	$Q \cong -\frac{UE\varphi}{Z}$	$P \cong \frac{U}{Z}[(E-U)\sin\theta - E\varphi\cos\theta]$

$$\overline{I_o} = \frac{E\angle\varphi - U\angle 0}{Z\angle\theta} = \frac{E}{Z}\angle(\varphi-\theta) - \frac{U}{Z}(-\theta) \tag{22.20}$$

$$\bar{Z} = R + jX \tag{22.21}$$

Also, active and reactive powers can be deriving from Eqs. (22.22) and (22.23).

$$P = \frac{U}{Z}[(E\cos\varphi - U)\cos\theta + E\sin\theta\sin\varphi] \tag{22.22}$$

$$Q = \frac{U}{Z}[(E\cos\varphi - U)\sin\theta - E\cos\theta\sin\varphi] \tag{22.23}$$

As the phase angle between the inverter bus voltage and PCC is negligible, Eqs. (22.22) and (22.23) can be simplified in the form of Eqs. (22.24) and (22.25) and Table 22.1.

$$P \cong \frac{U}{Z}[(E-U)\cos\theta + E\varphi\sin\theta] \tag{22.24}$$

$$Q \cong \frac{U}{Z}[(E-U)\sin\theta - E\varphi\cos\theta] \tag{22.25}$$

The relation between system impedance and the output active and reactive power of DG, the polar diagram of Figs. 22.6, 22.7 and 22.8 has been derived. The polar radius stands for active and reactive power and the radius is the power angle. It should be noted that only the shaded area is the acceptable in the real power system.

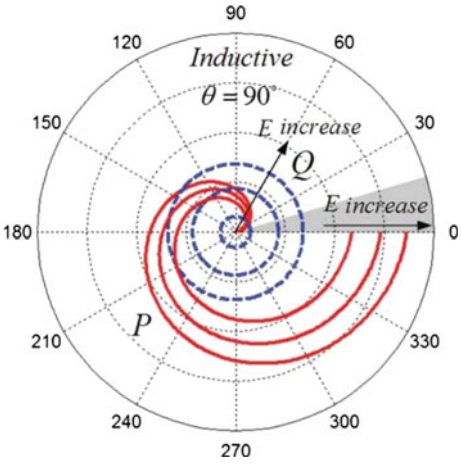

Fig. 22.6 Polar locus of active and reactive power—pure inductive case [18]

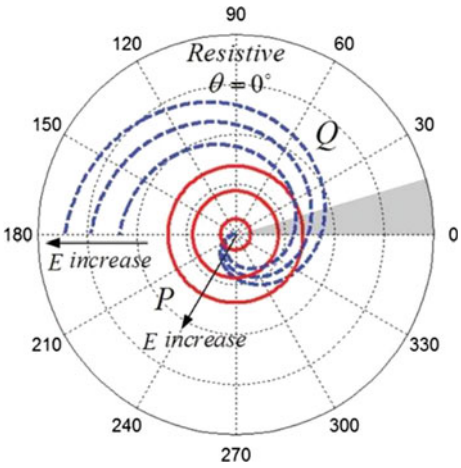

Fig. 22.7 Polar locus of active and reactive power—pure resistive case [18]

22.4.1 Pure Inductive Impedance

The active and reactive power curves have been shown in Fig. 22.6 for the pure inductive impedance. Both of them increase by increasing the inverter bus voltage. The active power is independent of phase angle but the reactive power increases by increasing the power phase angle.

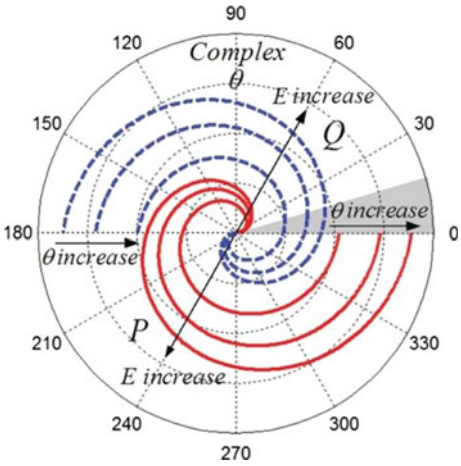

Fig. 22.8 Polar locus of active and reactive power—complex impedance case [18]

22.4.2 Pure Resistive Impedance

As shown in Fig. 22.7, the behavior of active and reactive power is opposite to the pure inductive case. Both active and reactive power increase by increasing the inverter bus voltage. The reactive power is independent of phase angle but the active power increases by increasing the power phase angle.

22.4.3 Complex Impedance

For the complex impedance, both the active and reactive powers increase by increasing the power phase angle. They move in the counter clockwise direction by increasing the power phase angle (Fig. 22.8). The behavior of powers in this case is more complicated than inductive or resistive cases. So designing the controller will be more complicated in this case.

In the case of equal resistance and reactance ($X = R$), the droop controllers can be defined by Eqs. (22.26) and (22.27).

$$\omega = \omega_0 - m_p \cdot (P - Q) \tag{22.26}$$

$$E = E_0 - n_Q \cdot (P + Q) \tag{22.27}$$

In [7], a PQV control method has been proposed to facilitate the simultaneous control of active and reactive power by voltage controlling the voltage of PCC. The proposed controller is presented in (22.28).

$$V = V_{ref} + (n_d \cdot P) + (m_d \cdot Q) \tag{22.28}$$

where, V_{ref} is the reference voltage of PCC, n_d and m_d are the droop coefficients of the active and reactive power. These coefficients are adaptively adjusted by a lookup table based on the PCC voltage.

To improve the dynamic behavior of the system, an advanced droop controller has been proposed in [26] as presented in Eqs. (22.29) and (22.30).

$$\varphi = -m \int_{-\infty}^{t} P d\tau - m_p P - m_d \frac{dP}{dt} \tag{22.29}$$

$$E = E^* - nQ - n_d \frac{dQ}{dt} \tag{22.30}$$

where, n_d is the coefficient of reactive power derivation. m, m_p and m_d are the coefficients of integrator, proportional and derivation of active power, respectively. These coefficients are dynamic and are derived for the small signal studies. Derivative part of the controller is added to the droop control to improve the controller speed. Also, it can reduce the circulating and startup currents in low voltage microgrids [27, 28]. Droop controllers are derived by Eqs. (22.31) and (22.32).

$$\omega = \omega^* + K_p\left(P_i - P_{i,ref}\right) + K_{pd}\frac{dP_i}{dt} \tag{22.31}$$

$$V_i = V_{ref} + K_Q\left(Q_i - Q_{i,ref}\right) + K_{qd}\frac{dQ_i}{dt} \tag{22.32}$$

where, K_{pd} and K_{qd} are adjusted by pole placement method to improve the performance of overall system.

22.5 Angle Droop Control

Power flow of a microgrid can be controlled by adjusting the phase angle of DG bus voltages [29]. Schematic diagram of a DG connected to the microgrid is shown in Fig. 22.9. The injected active and reactive power of DG to the grid has been derived by Eqs. (22.33) and (22.34).

$$p = \frac{V \times V_t \sin(\delta - \delta_t)}{X_f} \tag{22.33}$$

$$q = \frac{V^2 - V \times V_t \cos(\delta - \delta_t)}{X_f} \tag{22.34}$$

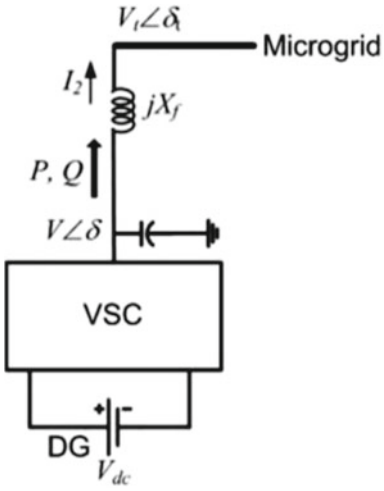

Fig. 22.9 DG connected to a microgrid by VSC [29]

As the phase angle between the output voltage of VSC and the PCC voltage is small, the active power is proportional to the phase angle. So similar to the frequency droop the following controllers can be derived.

$$\delta_i = \delta_{rated} - m_p \cdot P_i \tag{22.35}$$

$$E_i = E_{rated} - n_Q \cdot Q_i \tag{22.36}$$

where, E_{rated} and δ_{rated} are the nominal voltage and phase angle of DG, respectively. n_Q and m_p are the gains of active and reactive power gains, respectively. Phase droop can improve the power flow control of DGs and frequency stability considerably.

22.6 Droop Control Based on Virtual Impedance

The power quality of islanded microgids is highly damaged by nonlinear loads. Adjusting the virtual impedance by the droop controller can improve the impedance matching between DGs and the microgrid [25]. This leads to better dynamic performance of microgrid and reduces the circulating currents between DGs. Moreover, it is useful for harmonic reduction and appropriate power flow [24, 30].

The circuit diagram of two parallel DGs has been shown in Fig. 22.10. Phasor of voltages and impedances are defined as Eqs. (22.37)–(22.40).

$$|VO_1| = |VO_1|e^{j\theta 01} \tag{22.37}$$

$$|VO_2| = |VO_2|e^{j\theta 02} \tag{22.38}$$

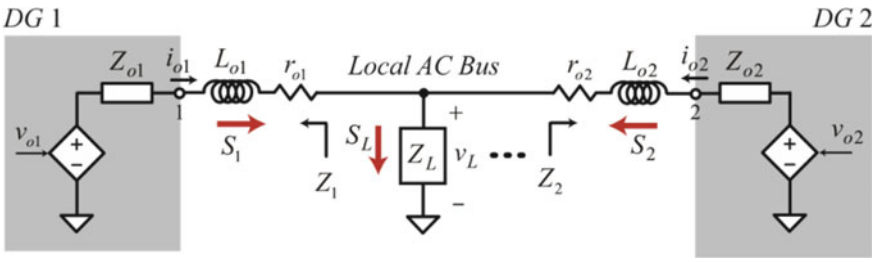

Fig. 22.10 Circuit diagram of connected DGs [30]

$$v_L = |v_L| e^{j\theta_L} \tag{22.39}$$

$$Z_1 = |Z_1| e^{(j<Z_1)} \tag{22.40}$$

Injected power from DG_1 to the AC bus can be derived by Eq. (22.41).

$$S_1 = V_{O1} I_O^* = \frac{|V_{O1}|^2}{Z_1} e^{(j<Z_1)} - \left(\frac{|V_{O1}||V_L|}{|Z_1|}\right) e^{(j<Z_1+\theta_{1L})} \tag{22.41}$$

where,

$$\theta_{1L} = \theta_{o1} - \theta_L \tag{22.42}$$

$$Z_1 = Z_{o1} + \omega_L + L_{01} e^{\frac{\pi}{2}} + r_{o1} \tag{22.43}$$

So, active and reactive powers are derived by Eqs. (22.44) and (22.45).

$$P_1 = \mathrm{Re}\{S_1\} = \left(\frac{|VO_1|^2}{|Z_1|} - \frac{|VO_1||vL|}{|Z_1|}\cos\theta_{1L}\right)\cos < Z_1 + \frac{|VO_1||V_L|}{|Z_1|}\sin\theta_{1L}\sin < Z_1 \tag{22.44}$$

$$Q_1 = \mathrm{Im}\{S_1\} = \left(\frac{|VO_1|^2}{|Z_1|} - \frac{|VO_1||vL|}{|Z_1|}\cos\theta_{1L}\right)\sin < Z_1 + \frac{|VO_1||V_L|}{|Z_1|}\sin\theta_{1L}\cos < Z_1 \tag{22.45}$$

The power transfer from DG1 to DG2 can be derived by Eqs. (22.46) and (22.47).

$$P_{12} = \left(\frac{|VO_1|^2}{|Z_{12}|} - \frac{|VO_1||VO_2|}{|Z_{12}|}\cos\theta_{12}\right)\cos < Z_{12}$$

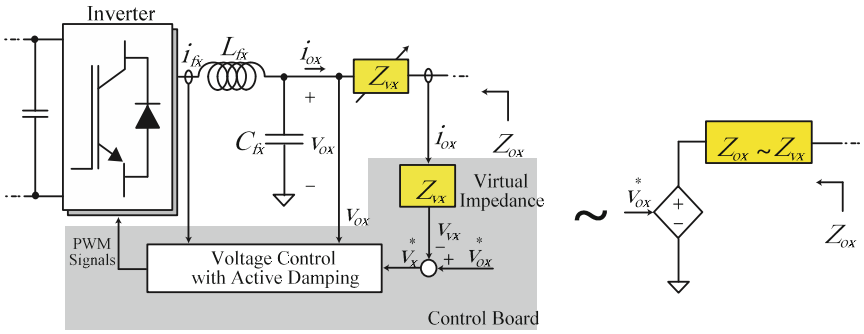

Fig. 22.11 Virtual impedance of DG [30]

$$+ \frac{|VO_1||VO_2|}{|Z_{12}|} \sin\theta_{12} \sin < Z_{12} \tag{22.46}$$

$$Q_{12} = \left(\frac{|VO_1|^2}{|Z_{12}|} - \frac{|VO_1||VO_2|}{|Z_{12}|} \cos\theta_{12} \right) \sin < Z_{12}$$
$$+ \frac{|VO_1||VO_2|}{|Z_{12}|} \sin\theta_{12} \cos < Z_{12} \tag{22.47}$$

Power transfer between DGs is not acceptable, because it leads to power oscillations and power losses. The internal impedance values of DG1 and DG2, Z_{o1} and Z_{o2} in Fig. 22.10, can be adjusted by control mechanism called virtual impedance.

It can be reduced by adjusting the virtual impedances of DGs. virtual impedance is the internal impedance of DGs that can be adjusted by the switching control of their inverter, as shown in Fig. 22.11.

The virtual impedance (Z_{vx}) can be derived by Eq. (22.48).

$$V_x^* = V_{ox}^* - V_{vx} = V_{ox}^* - Z_{vx} i_{ox} \tag{22.48}$$

As Z_{vx} is approximately equal to Z_{ox}, it can be presented in the form of Eq. (22.49) in the Laplace domain.

$$Z_{vx}(S) = SL_{vx} \tag{22.49}$$

where, S is the Laplace operator and L_{vx} is the inductance of the virtual impedance. So the voltage droop is defined by Eq. (22.50).

$$V_{vx}(S) = SL_{vx} i_{ox} \tag{22.50}$$

For the real implementation of Eq. (22.50), a real pole should be added to the differentiator as a low-pass filter, as shown in Eq. (22.51).

$$V_{vx}(S) = L_{vx}\frac{\omega_v s}{s+\omega_v} i_{ox} \tag{22.51}$$

where, ω_v is the cut-off frequency of the low-pass filter [30].

22.7 Droop Control Based on Virtual Frame

This control method is based on the definition of a virtual reference frame for voltage and frequency to decouple the active and reactive control in microgrid. In the pure inductive microgrids, active power can be controlled by the frequency (or phase angle) of DG inverter and the reactive power can be controlled by the output voltage of the inverter. These relations have been derived by Eqs. (22.52)–(22.59) based on the circuit diagram of Fig. 22.12 [31].

$$\begin{aligned} S &= P + jQU_1 \\ I^* &= U_1\left(\frac{U_1 - U_2}{Z}\right)^* \\ &= U_1\left(\frac{U_1 - U_2 e^{j\delta}}{Z e^{-j\theta}}\right)^* \\ &= \frac{U_1^2}{Z}e^{j\theta} - \frac{U_1 U_2}{Z}e^{j(\theta+\delta)} \end{aligned} \tag{22.52}$$

$$P = \frac{U_1^2}{Z}\cos\theta - \frac{U_1 U_2}{Z}\cos(\theta+\delta) \tag{22.53}$$

$$Q = \frac{U_1^2}{Z}\sin\theta - \frac{U_1 U_2}{Z}\sin(\theta+\delta) \tag{22.54}$$

where,

$$Ze^{j\theta} = R + jX \tag{22.55}$$

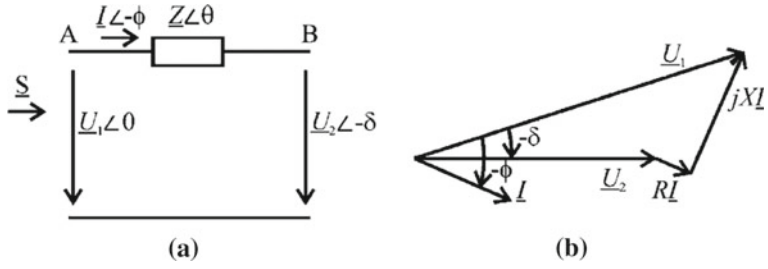

Fig. 22.12 Circuit and phasor diagram to calculate power transfer [31]

Substituting Z in the previous equations leads to Eqs. (22.56)–(22.59).

$$P = \frac{U_1^2}{R^2 + X^2}[R(U_1 - U_2\cos\delta) + XU_2\sin(\delta)] \tag{22.56}$$

$$P = \frac{U_1^2}{R^2 + X^2}[R(U_1 - U_2\cos\delta) + XU_2\sin(\delta)] \tag{22.57}$$

$$U_2\sin(\delta) = \frac{XP - RQ}{U_1} \tag{22.58}$$

$$U_1 - U_2\cos\delta = \frac{RP + XQ}{U_1} \tag{22.59}$$

For the transmission lines with $X \gg R$, R can be neglected and if δ is considerably small (near zero), then, $\sin(\delta) = \delta$ and $\cos(\delta) = 1$. With these assumptions, Eqs. (22.58) and (22.59) can be rewritten as follows.

$$\delta \cong \frac{XP}{U_1U_2} \tag{22.60}$$

$$U_1 - U_2 \cong \frac{XQ}{U_1} \tag{22.61}$$

It can be seen that phase angle is proportional to the active power and the voltage difference is dependent to the reactive power. It means that phase angle and inverter voltage can be controlled by active and reactive power, respectively. It should be noted that the proposed droop control is appropriate when the line resistance is considerably smaller than the line inductance. The linear transformation matrix of Eq. (22.62) can be used to overcome this shortcoming of droop control.

$$\begin{bmatrix} P' \\ Q' \end{bmatrix} = T\begin{bmatrix} P \\ Q \end{bmatrix} = \begin{bmatrix} \sin\theta & -\cos\theta \\ \cos\theta & \sin\theta \end{bmatrix}\begin{bmatrix} P \\ Q \end{bmatrix} \tag{22.62}$$

Applying this transformation to Eqs. (22.56) and (22.57) results in:

$$\sin\delta = \frac{ZP'}{U_1U_2} \tag{22.63}$$

$$U_1 - U_2\cos\delta = \frac{ZQ'}{U_1} \tag{22.64}$$

For the small phase angle (δ), it is proportional to the transformed active power (P') and the voltage difference is dependent to the transformed reactive power (Q'). So, these equations can be used to define the frequency and voltage droops, as shown in Fig. 22.13.

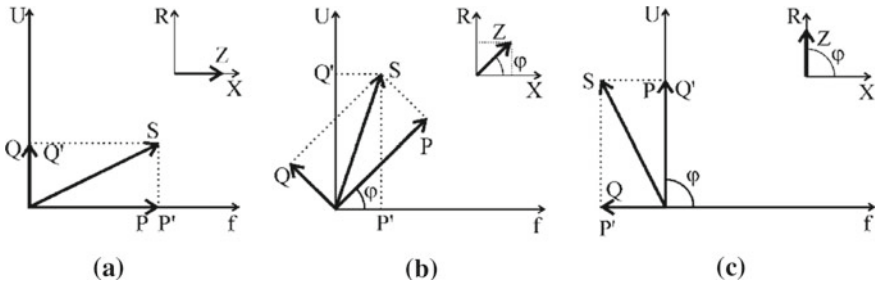

Fig. 22.13 Effect of transformed powers on frequency and voltage for different *R*/*X* [31]

For the pure inductive lines:

$$P' \approx P \tag{22.65}$$

$$Q' \approx Q \tag{22.66}$$

For the pure resistive lines, Eqs. (22.67) and (22.68) can be used.

$$P' \approx -Q \tag{22.67}$$

$$Q' \approx P \tag{22.68}$$

So the droop controller can be derived by Eqs. (22.69) and (22.70).

$$f - f_0 = -k_p\left(P' - P'_0\right) = -k_p\frac{X}{Z}(P - P_0) + k_p\frac{R}{Z}(Q - Q_0) \tag{22.69}$$

$$U_1 - U_0 = -k_q\left(Q' - Q'_0\right) = -k_q\frac{R}{Z}(P - P_0) - q\frac{R}{Z}(Q - Q_0) \tag{22.70}$$

22.8 Adaptive Voltage Droop Control

VSCs with the conventional voltage droop controller allocate reactive power between DGs of the microgrid. The accuracy of power flow depends on the parameters of the system and controllers [32]. To study the dependency, a simple microgrid is considered in Fig. 22.14 [32].

The relation between bus voltage and DG voltage is derived by Eq. (22.71).

$$V_i\angle\alpha_i = E_i\angle\delta_i - Z_iI_i\angle - \theta_i, \quad i = 1, 2 \tag{22.71}$$

As stated before, the conventional droop defines by Eqs. (22.72) and (22.73).

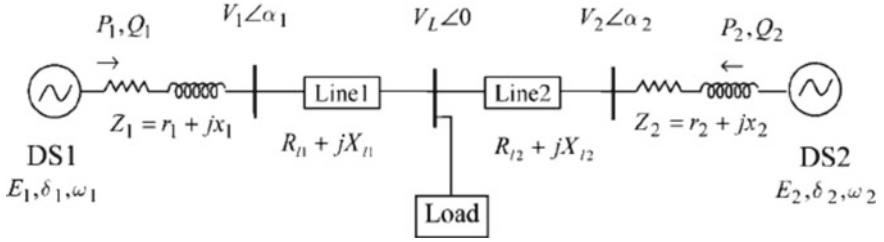

Fig. 22.14 Circuit diagram of a simple microgrid [32]

$$\omega = \omega_0 - m_p P \tag{22.72}$$

$$E = E_0 - n_q Q \tag{22.73}$$

Substituting Eqs. (22.72) and (22.73) by Eq. (22.71) leads to the following equation [33].

$$V_i\angle\alpha_i = \left(E_0 - n_{qi}Q_i\right)\angle\delta_i - Z_i I_i\angle\theta - \theta_i \tag{22.74}$$

By defining $Z_i = r_i + jX_i$, $\gamma_i = \alpha_i + \theta_i$ and assuming $\delta_i - \alpha_i \cong 0$, V_i can be derived by Eq. (22.75).

$$V_i = E_0 - n_{qi}Q_i - r_i I_i \cos\gamma_i - x_i I_i \sin\gamma_i \tag{22.75}$$

Based on the active and reactive powers, V_i can be written by Eq. (22.76) [33].

$$V_i = E_0 - n_{qi}Q_i - \frac{r_i P_i}{E_i} - \frac{x_i Q_i}{E_i} \tag{22.76}$$

The voltage magnitude of ith bus depends on the control parameters n_{qi} and E_o, active and reactive power of VSC and the connection impedance. To reduce the effect of these parameters, the voltage drop on the connection impedance is added to the voltage reference of the VSC. So the conventional E-Q droop modifies by Eqs. (22.77) and (22.78).

$$E_i = E_0 + \left(\frac{r_i P_i + x_i Q_i}{E_0}\right) - n_{q_i} Q_i \tag{22.77}$$

$$D_i(P_i \cdot Q_i) = D_{Qi} + m_{Qi}Q_i^2 + m_{pi}P_i^2 \tag{22.78}$$

where, D_i, m_{Qi} and m_{Pi} are droop coefficients. Although this method reduces the effect of active control, high loading and different parameters of microgrid, the need to know some parameters of the system is its weakness.

The reference of VSC voltage can be adaptively adjusted based on the active and reactive powers by the droop control of Eq. (22.79).

$$E_i = \left(E_0 + \frac{r_i P_i}{E_{0i}}\right) - \left(n_{qi} - \frac{X_i}{E_0}\right) Q_i \tag{22.79}$$

The first part of E_i varies from E_o (no load condition) to $E_0 + r_i P_i / E_0$ and the second part (voltage droop coefficient) varies from n_{qi} to $n_{qi} - x_i / E_0$. It means that the slope of droop controller varies in different operating conditions. This controller removes the effect of the connection impedance between VSC and PCC [32].

22.9 Simulation Results

Figure 22.15 shows a typical microgrid including two distributed generations (DG1 and DG2) to assess the conventional droop, virtual impedance and coupling in a medium voltage distribution network. The microgrid is a three-wire distribution network, operated in the islanded mode. It is assumed that the load 1 is fixed and load 2 is connected to the microgrid at $t = 2.5$ s. The general information of the microgrid and its components are depicted in Table 22.2. The active and reactive sharing of DGs are illustrated in Figs. 22.16, 22.17, 22.18, 22.19, 22.20 and 22.21.

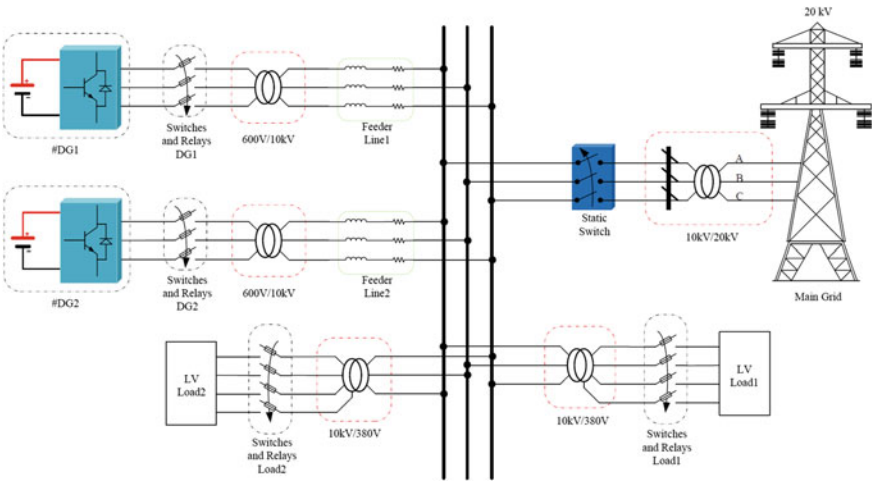

Fig. 22.15 Configuration of a typical MV microgrid

Table 22.2 General information of the MV microgrid

General information			
Parameter		Value	
Nominal voltage (rms, L-L)		10 kV	
Allowable voltage range (%)		±5	
Frequency		60 Hz	
Allowable frequency range (%)		±1	
Feeder and branches			
Voltage level	*R* (Ω/km)	*X* (Ω/km)	*R*/*X* (p.u.)
MV (10 kV)	0.161	0.19	0.85
Feeder DG1: 2 km, Feeder DG2: 6 km			
DG units			
DG No.	Technology		Capacity
DG1	Fuel cell		1.5 MW
DG2	Photovoltaic with battery		1.5 MW
Load			
Load No.	Type	Nominal active power	Power factor (cosφ)
Load 1	3×ϕ	100 kW	0.85 lag
Load 2	3×ϕ	100 kW	0.85 lag

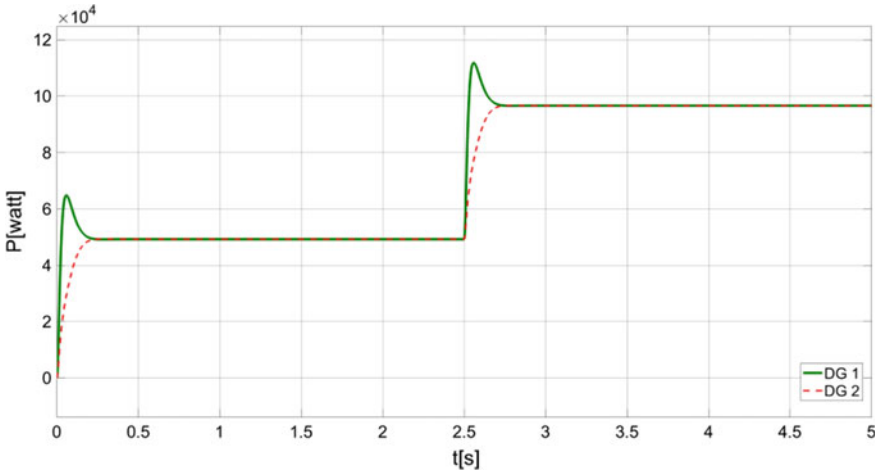

Fig. 22.16 Active power sharing with conventional droop method

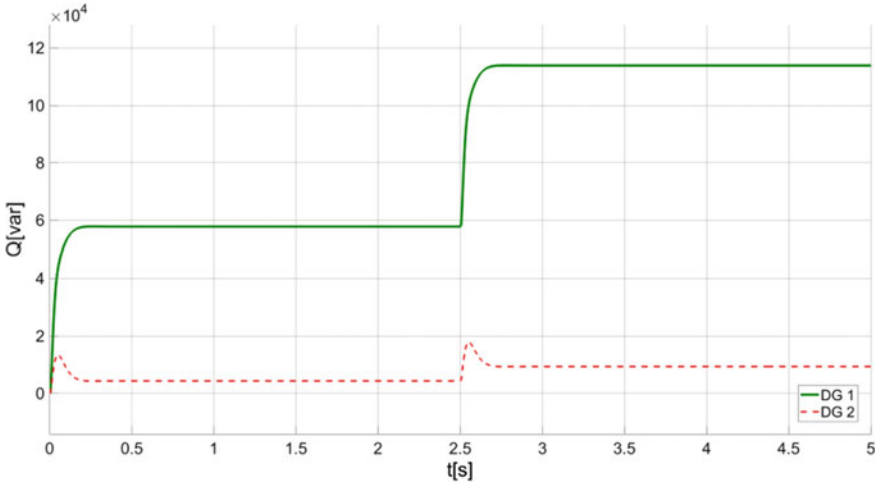

Fig. 22.17 Reactive power sharing with conventional droop method

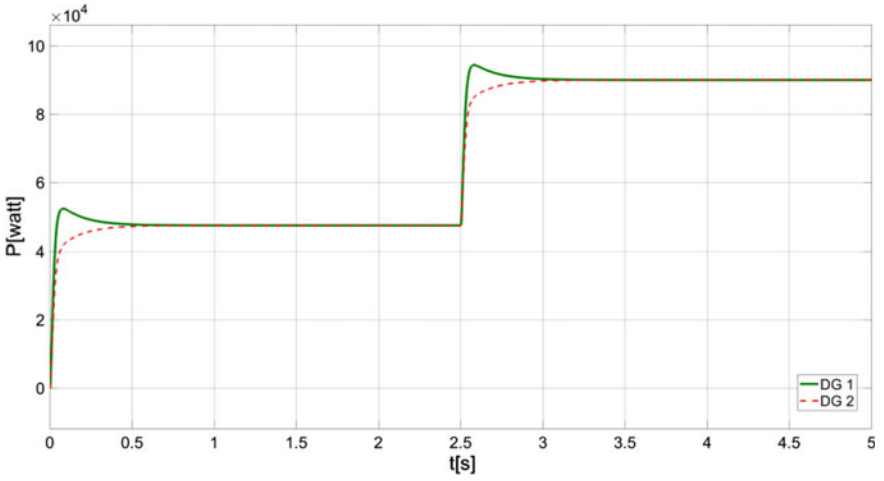

Fig. 22.18 Active power sharing among DG units by applying virtual impedance in the conventional droop

22.9.1 Conventional Droop

Figure 22.16 shows that due to the interdependency between active power and frequency in the conventional droop, DG units with equal capacity have to inject same active power. As expected, the sharing of reactive power through conventional droop

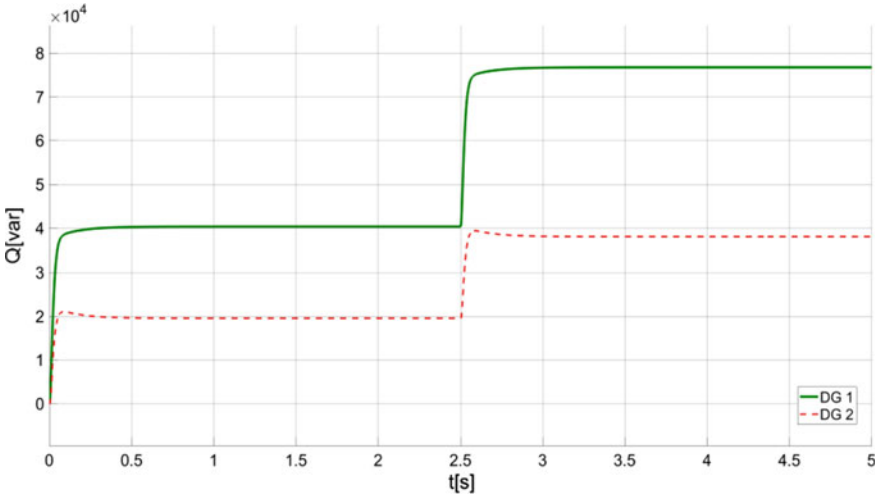

Fig. 22.19 Reactive power sharing among DG units by applying virtual impedance in the conventional droop

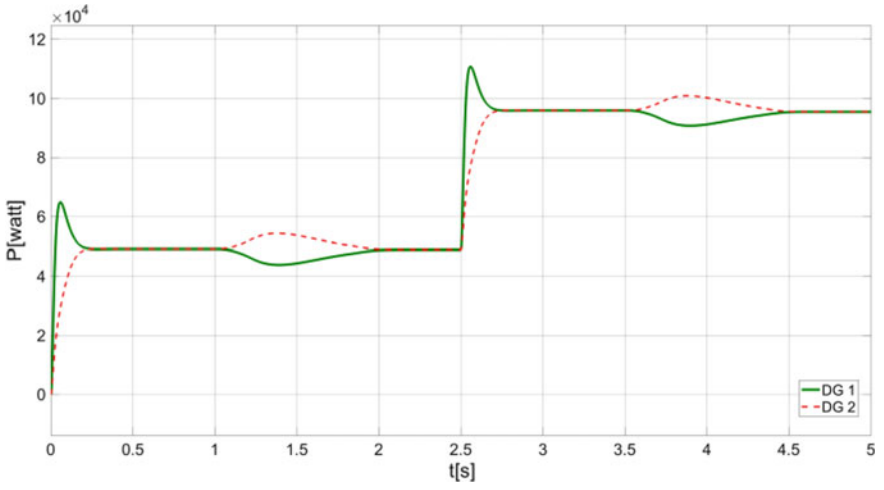

Fig. 22.20 The effect of decentralized reactive power sharing on conventional active power sharing

is dependent on the feeder impedance DG and local load. Thus, as shown in Fig. 22.17, the higher load current, the higher feeder voltage drops and the greater lack of reactive power sharing among DG units.

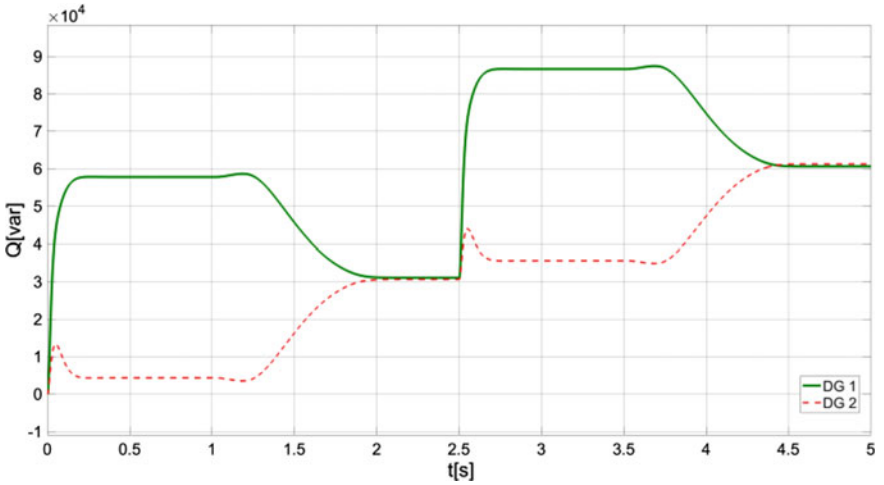

Fig. 22.21 The effect of decentralized reactive power sharing on conventional reactive power sharing

22.9.2 Effects of the Virtual Impedance on the Conventional Droop

By applying appropriate virtual impedance, it is possible to get better results in comparison with the conventional droop. Figures 22.18 and 22.19 shows the result of active and reactive power sharing among DG units respectively. It is observed that difference between the reactive power sharing in Fig. 22.17 has been reduced in Fig. 22.19.

22.9.3 Effects of the Reactive Power Compensation on the Conventional Droop

This approach has an appropriate active and reactive power sharing for the conventional droop. Figures 22.20 and 22.21 show the result of active and reactive power sharing between DG1 and DG2 respectively. It is observed that after applying the decentralized reactive power sharing, the active and reactive power of both DGs follow the same value and an equal power sharing obtain.

22.9.4 *Reverse Droop—LV Microgrid*

Figure 22.22 shows a typical microgrid including five (DGs) to analysis the reverse droop in low voltage (LV) distribution network (380 V). The microgrid is a four-wire distribution network, which is operated in the islanded mode. The wiring is based on underground cables and it is assumed that all loads are balanced three-phase. DG units are dispatchable and power electronic interface based with total capacity equal to 140 kW. Each DG has an inverter and a local controller consists of reverse droop, inner voltage and current loop. A LC filter has been set in the output of the inverter to eliminate switching harmonics. Table 22.3 presents the general information of the microgrid shown in Fig. 22.22. It is assumed that load 1 is fixed and connected to the microgrid, load 2 is disconnected from the microgrid at $t = 0.5$ s, while load 3 is connected at $t = 1$ s.

In the reverse droop, the reactive power and frequency has interdependency and therefore the reactive power of DG units with equal capacity follow a same value after any change. Figure 22.23 shows the reactive power sharing among DG units

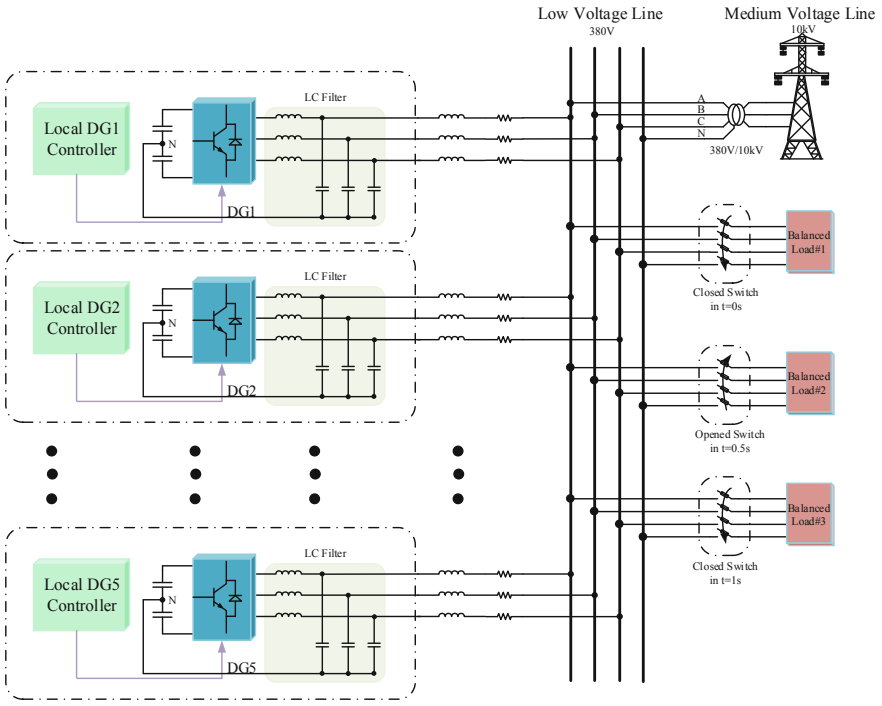

Fig. 22.22 Configuration of a typical MV microgrid

Table 22.3 General information of LV microgrid

General information			
Parameter		Value	
Nominal voltage (rms, L-L)		380 V	
Allowable voltage range (%)		±5	
Frequency		60 Hz	
Allowable frequency range (%)		±1	
Feeder and branches			
Voltage level	*R* (Ω/km)	*X* (Ω/km)	*R*/*X* (p.u.)
LV (380 V)	0.642	0.083	7.7
Feeder DG1: 2 km, Feeder DG2: 6 km, Feeder DG3: 3 km, Feeder DG 4: 9 km, Feeder DG5: 2.5 km			
DG units			
DG No.	Technology		Capacity
DG1	Fuel cell		35 kW
DG2	Photovoltaic with battery		35 kW
DG3	Photovoltaic with battery		35 kW
DG4	Photovoltaic with battery		17.5 kW
DG5	Fuel cell		17.5 kW
Load			
Load No.	Type	Nominal active power	Power factor (cosφ)
Load 1	3×ϕ	10 kW	0.85 lag
Load 2	3×ϕ	10 kW	0.85 lag
Load 3	3×ϕ	20 kW	0.85 lag

through reverse droop. It is observed that DG 1, 2 and 3 with equal capacity has the same reactive power generation. Similarly, DG 4 and 5 with half capacity of the others proportionally participate in reactive power sharing. Reactive power sharing is performed appropriately after any change in the microgrid at 0.5 and 1 s. None of DG units injects equal active power into the microgrid due to the different impedance between DGs and loads. Figure 22.24 shows the difference between values of active power generation which increases by increasing the load current. The effects of load change on the frequency of the microgrid are shown in Fig. 22.25.

22.10 Conclusion

Each of the mentioned droop controllers has some benefits and shortcomings. The common benefits of droop controllers are Local implementation, no need to communication systems, easy expansion, acceptable reliability and low investment cost. Fre-

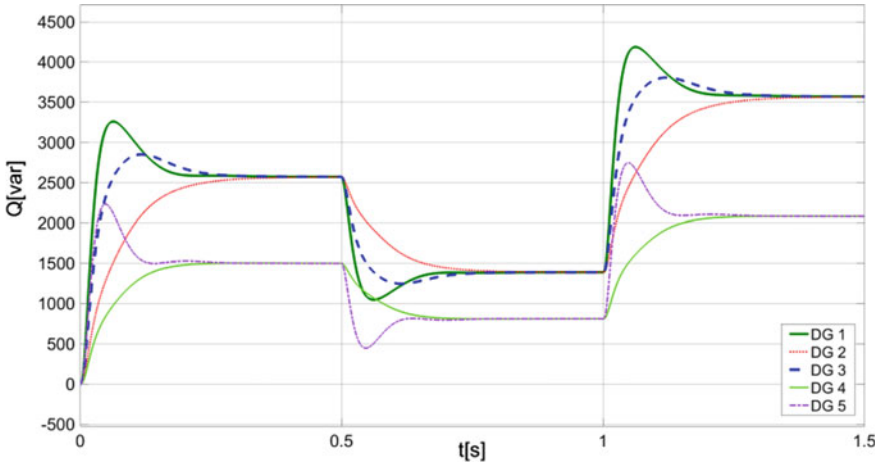

Fig. 22.23 Reactive power sharing among DG units based on reverse droop

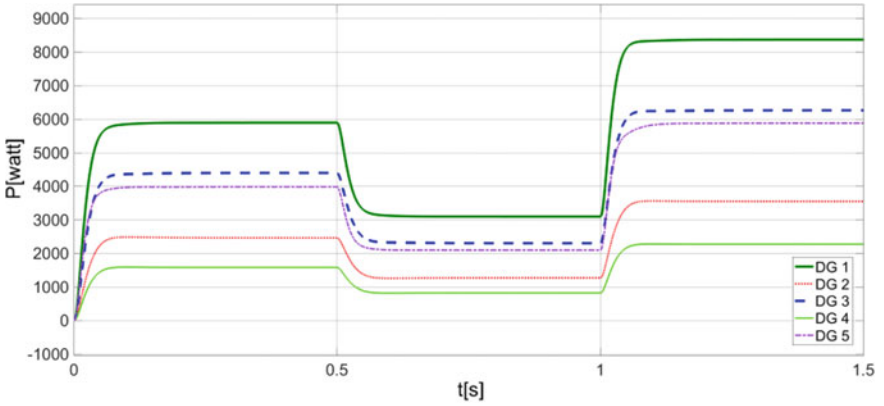

Fig. 22.24 Active power sharing among DG units based on reverse droop

quency deviation, slow dynamic response and circulating current are some shortcomings of droop controllers. Improving the performance of droop controllers, improves the performance of the microgrids considerably. Some advanced methods like multi agent systems and fractional order controllers are good candidates to modify droop controllers.

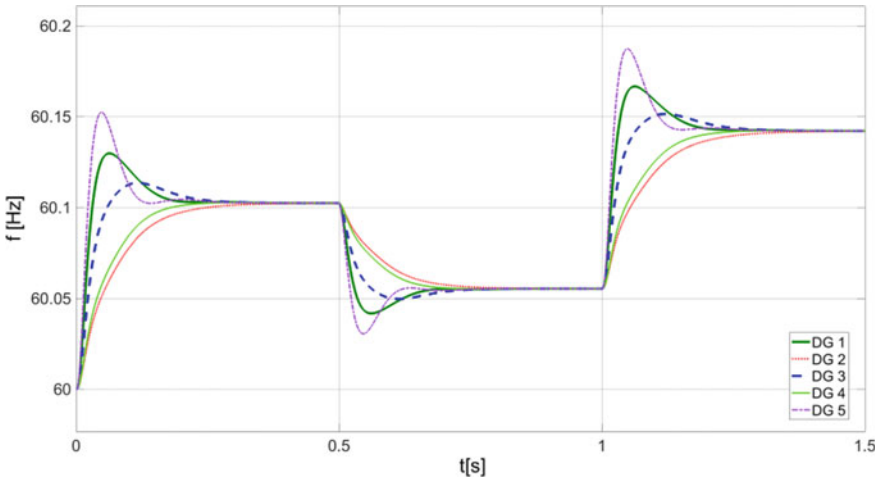

Fig. 22.25 Load change effects on the frequency of the microgrid

References

1. M.C. Chandrokar, D.M. Divan, B. Banerjee, Control of distributed UPS systems, in *Proceedings of 1994 Power Electronics Specialist Conference—PESC'94*, Taipei, Taiwan, vol. 1, pp. 197–204 (1994)
2. M.C. Chandorkar, D.M. Divan, R. Adapa, Control of parallel connected inverters in standalone AC supply systems. IEEE Trans. Ind. Appl. **29**(1), 136–143 (1993)
3. L. Lu, C. Chu, Consensus-based droop control synthesis for multiple DICs in isolated microgrids, in *IEEE Power & Energy Society General Meeting*, Denver, CO, pp. 1–10 (2015)
4. J. He, Y.W. Li, An enhanced microgrid load demand sharing strategy. IEEE Trans. Power Electron. **27**(9), 3984–3995 (2012)
5. A. Tuladhar, H. Jin, T. Unger, K. Mauch, Parallel operation of single phase inverter modules with no control interconnections, in *Proceedings of APEC 97—Applied Power Electronics Conference*, Atlanta, GA, USA, vol. 1, pp. 94–100 (1997)
6. A. Tuladhar, H. Jin, T. Unger, K. Mauch, Control of parallel inverters in distributed AC power systems with consideration of line impedance effect. IEEE Trans. Ind. Appl. **36**(1), 131–138 (2000)
7. J.C. Vasquez, J.M. Guerrero, A. Luna, P. Rodriguez, R. Teodorescu, Adaptive droop control applied to voltage-source inverters operating in grid-connected and islanded modes. IEEE Trans. Industr. Electron. **56**(10), 4088–4096 (2009)
8. Y.W. Li, C. Kao, An accurate power control strategy for power-electronics-interfaced distributed generation units operating in a low-voltage multibus microgrid. IEEE Trans. Power Electron. **24**(12), 2977–2988 (2009)
9. M.A. Mahmud, M.J. Hossain, H.R. Pota, A.M.T. Oo, Robust nonlinear distributed controller design for active and reactive power sharing in islanded microgrids. IEEE Trans. Energy Convers. **29**(4), 893–903 (2014)
10. B. John, A. Ghosh, F. Zare, Load sharing in medium voltage islanded microgrids with advanced angle droop control. IEEE Trans. Smart Grid **9**(6), 6461–6469 (2018)
11. D. Choi, J. Park, S.H. Lee, Virtual multi-slack droop control of stand-alone microgrid with high renewable penetration based on power sensitivity analysis. IEEE Trans. Power Syst. **33**(3), 3408–3417 (2018)

12. S. Peyghami, H. Mokhtari, P.C. Loh, P. Davari, F. Blaabjerg, Distributed primary and secondary power sharing in a droop-controlled LVDC microgrid with merged AC and DC characteristics. IEEE Trans. Smart Grid **9**(3), 2284–2294 (2018)
13. F. Cingoz, A. Elrayyah, Y. Sozer, Optimized settings of droop parameters using stochastic load modeling for effective DC microgrids operation. IEEE Trans. Ind. Appl. **53**(2), 1358–1371 (2017)
14. Q. Peng, T. Liu, S. Wang, Y. Qiu, X. Li, B. Li, Determination of droop control coefficient of multi-terminal VSC-HVDC with system stability consideration. IET Renew. Power Gener. **12**(13), 1508–1515 (2018)
15. D. Shanxu, M. Yu, X. Jian, K. Yong, C. Jian, Parallel operation control technique of voltage source inverters in UPS, in *IEEE International Conference on Power Electronics and Drive Systems. PEDS'99*, Hong Kong, vol. 2, pp. 883–887 (1992)
16. K. Siri, C.Q. Lee, T. Wu, Current distribution control for parallel connected converters, II. IEEE Trans. Aerosp. Electron. Syst. **28**(3), 841–851 (1992)
17. J.F. Chen, C.L. Chu, Combination voltage-controlled and current-controlled PWM inverters for UPS parallel operation. IEEE Trans. Power Electron. **10**(5), 547–558 (1995)
18. W. Yao, M. Chen, J. Matas, J.M. Guerrero, Z. Qian, Design and analysis of the droop control method for parallel inverters considering the impact of the complex impedance on the power sharing. IEEE Trans. Industr. Electron. **58**(2), 576–588 (2011)
19. Y. Pei, G. Jiang, X. Yang, Z. Wang, Auto-master-slave control technique of parallel inverters in distributed AC power systems and UPS, in *IEEE 35th Annual Power Electronics Specialists Conference*, Aachen, Germany, vol. 3, pp. 2050–2053 (2004)
20. J. Tan, H. Lin, J. Zhang, J. Ying, A novel load sharing control technique for paralleled inverters, in *IEEE 34th Annual Conference on Power Electronics Specialist (PESC '03)*, Acapulco, Mexico, vol. 3, pp. 1432–1437 (2003)
21. U.B. Tayab, M.A.B. Roslan, L.J. Hwai, M. Kashif, A review of droop control techniques for microgrid. Renew. Sustain. Energy Rev. **76**, 717–727 (2017)
22. X. Hou, Y. Sun, W. Yuan, H. Han, C. Zhong, J.M. Guerrero, Conventional P-ω/QV droop control in highly resistive line of low-voltage converter-based ac microgrid. Energies **9**(11), 943 (2016)
23. M. Kosari, S.H. Hosseinian, Decentralized reactive power sharing and frequency restoration in islanded microgrid. IEEE Trans. Power Syst. **32**(4), 2901–2912 (2017)
24. J.M. Guerrero, L. Garcia de Vicuna, J. Matas, M. Castilla, J. Miret, Output impedance design of parallel-connected UPS inverters with wireless load-sharing control. IEEE Trans. Industr. Electron. **52**(4), 1126–1135 (2005)
25. H. Han, X. Hou, J. Yang, J. Wu, M. Su, J.M. Guerrero, Review of power sharing control strategies for islanding operation of AC microgrids. IEEE Trans. Smart Grid **7**(1), 200–215 (2016)
26. J.M. Guerrero, L.G. de Vicuna, J. Matas, M. Castilla, J. Miret, A wireless controller to enhance dynamic performance of parallel inverters in distributed generation systems. IEEE Trans. Power Electron. **19**(5), 1205–1213 (2004)
27. G. Yajuan, W. Weiyang, G. Xiaoqiang, G. Herong, An improved droop controller for grid-connected voltage source inverter in microgrid, in *The 2nd International Symposium on Power Electronics for Distributed Generation Systems*, Hefei, pp. 823–828 (2010)
28. Y.A.I. Mohamed, E.F. El Saadany, Adaptive decentralized droop controller to preserve power sharing stability of paralleled inverters in distributed generation microgrids. IEEE Trans. Power Electron. **23**(6), 2806–2816 (2008)
29. R. Majumder, A. Ghosh, G. Ledwich, F. Zare, Angle droop versus frequency droop in a voltage source converter based autonomous microgrid, in *IEEE Power & Energy Society General Meeting*, Calgary, AB, pp. 1–8 (2009)
30. Y.O. Choi, J. Kim, Output impedance control method of inverter-based distributed generators for autonomous microgrid. Energies **10**(7), 904 (2017)
31. K. de Brabandere, B. Bolsens, J. Van den Keybus, A. Woyte, J. Driesen, R. Belmans, A voltage and frequency droop control method for parallel inverters. IEEE Trans. Power Electron. **22**(4), 1107–1115 (2007)

32. E. Rokrok, M.E.H. Golshan, Adaptive voltage droop scheme for voltage source converters in an islanded multibus microgrid. IET Gener. Transm. Distrib. **4**(5), 562–578 (2010)
33. A. Bidram, A. Davoudi, Hierarchical structure of microgrids control system. IEEE Trans. Smart Grid **3**(4), 1963–1976 (2012)